

MEASUREMENT OF THERMAL NEUTRON CROSS SECTION AND RESONANCE INTEGRAL FOR $^{139}\text{La}(n,\gamma)^{140}\text{La}$ REACTION BY ACTIVATION METHOD USING CADMIUM RATIOS

Yücel, H. , Karadağ, M.** , Çetiner, M.A.* , Tan, M.** And Özmen, A.***

* Ankara Nuclear Research and Training Center (ANRTC), 06100 Beşevler, Ankara, Turkey

** Gazi University, Gazi Education Faculty, Art and Science Faculty, Physics Department, 06500 Teknikokullar, Ankara, Turkey

Abstract

Thermal neutron cross section and resonance integral for the $^{139}\text{La}(n,\gamma)^{140}\text{La}$ reaction was measured by the activation method. The experimental samples with and without a cylindrical Cd shield case in 1 mm wall thickness were irradiated in an isotropic neutron field of the ^{241}Am -Be neutron source. The extent of the non-ideality of the epithermal neutron spectrum (i.e., α -shaping factor for $1/E^{1+\alpha}$ epithermal distribution) at the sample irradiation position was experimentally determined by the two-detector (Au and W foils) method, and it was found to be 0.560 ± 0.002 . The induced activities in the samples were measured by high resolution γ -ray spectrometry with a calibrated n-type Ge detector. Thermal neutron cross section for 2200 m/s neutrons and resonance integral for the $^{139}\text{La}(n,\gamma)^{140}\text{La}$ reaction has been obtained relative to the reference values, $\sigma_0 = 13.3 \pm 0.1$ b and $I_0 = 14.0 \pm 0.3$ b for the $^{55}\text{Mn}(n,\gamma)^{56}\text{Mn}$ reaction as a single comparator. The results corrected for gamma attenuation, thermal neutron and resonance neutron self-shielding effects and the effect of α -shaping factor on the resonance integral value of the (n,γ) reactions. For the conversion of the measured infinite dilution resonance integral, $I(\alpha)$ to the I_0 for $1/E$ ideal epithermal neutron spectrum, the concept of effective resonance energy, \bar{E}_r described by De Corte for the Ryves' method [1] has been used. By defining Cd cut-off energy 0.55 eV, the results obtained were: $\sigma_0 = 9.27 \pm 0.37$ b and $I_0 = 12.16 \pm 0.60$ b for the $^{139}\text{La}(n,\gamma)^{140}\text{La}$ reaction. These results are discussed and compared with previous measurements and the evaluated data in JEF-2.2, IAEA and JENDL-3.2. Thermal neutron cross section for $^{139}\text{La}(n,\gamma)^{140}\text{La}$ reaction is in good agreement with the recent measurements. There existed the discrepancies between present results and some of old experimental data for thermal cross section and resonance integral for this reaction is within about 6-40%.

1. Introduction

A knowledge of thermal neutron cross-section and resonance integral cross-section for lanthanum (La), which is as a rare earth element from the lanthanides is important for thermal or epithermal neutron activation analysis. Both resonance integrals and thermal cross sections are required in the theoretical and experimental studies concerning in experimental reactor physics and in checking nuclear resonance parameters within the interaction of neutrons with matter. For most isotopes a wide range of reported values exists, so that often a resonance integral is not known within 20%, making it of little practical use[1]. It is also apparent the uncertainties quoted for many measurements are poorly defined and unrealistically small. The measured thermal neutron cross-sections for $^{139}\text{La}(n,\gamma)^{140}\text{La}$ reaction in the literature are usually consistency, but some of old experimental thermal neutron cross-sections and resonance integrals for this reaction differ about 6-30% from each other due to the known problems such as the separation of the response of the nuclide to be activated to intermediate neutrons, much larger self-shielding for epithermal(intermediate energy) neutrons (from cadmium cut-off energy 0.55 eV to about 0.1 MeV), and the perturbation of the response corresponding to the resonance peak by the contribution of the $1/v$ region of thermal neutron cross section. As the required precision of measurements increases, it becomes desirable to provide more consistent resonance integral data.

Methods of measurement for thermal cross section for thermal neutrons and the resonance integral for epithermal neutrons are the pile reactivity and the activation technique[2] The first method implies reactivity measurements with a reactor oscillator, while the second method implies foil activations to compare cadmium ratios for foils of the materials of interest to cadmium ratio of foils of a reference material, for which usually gold ($\sigma_0=98.65 \pm 0.09$ b, $I_0=1550 \pm 28$ b) is employed [3]. Since there are sufficient number of internationally accepted accurate values for the thermal neutron cross section (known to $\pm 0.75\%$) and resonance integral (known to $\pm 2\%$) for $^{55}\text{Mn}(n,\gamma)^{56}\text{Mn}$, we have used Mn monitor instead of standard Au monitor. In addition, the $^{55}\text{Mn}(n,\gamma)^{56}\text{Mn}$ reaction can be chosen as a suitable monitor in this experiment because the value of the resonance integral for $^{55}\text{Mn}(n,\gamma)^{56}\text{Mn}$ monitor reaction is in the same order with that for $^{139}\text{La}(n,\gamma)^{140}\text{La}$ and the characteristic-prominent resonances in the epithermal region for ^{55}Mn and ^{139}La are far from 0.55 eV cadmium cut-off energy, which is in a cylindrical Cd box (height/diameter=2) with a wall thickness of 1mm, according to the definition of E.A.N.D.C[4].

The purpose of this study is to measure the thermal neutron cross section and resonance integral for the $^{139}\text{La}(n,\gamma)^{140}\text{La}$ reaction by an activation technique using cadmium ratios, relative to a single standard material, manganese in an isotropic neutron field by $^{241}\text{Am-Be}$ neutron source.

2. Experimental

In the present measurements, the oxide forms of the elements(La and Mn) were diluted by more 90% using Al_2O_3 with low absorption cross section($\sigma_a = 0.23$ b) so as to minimize errors due to neutron self shielding effect. Then the samples were irradiated in an isotropic neutron field of the three 592 GBq ^{241}Am -Be neutron sources. The geometrical configuration of the neutron sources immersed in paraffin moderator shielded with lead as a neutron irradiation unit, installed at Ankara Nuclear Research and Training Center (ANRTC), is shown in Fig 1. The oxide forms of the analytical grade samples to be activated were filled in the polystyrene tubes (height/diameter ≈ 2) with 1 mm wall thickness. They were exposed to the neutrons in a fixed position in the irradiation hole(labeled no.1 in Fig1) of very large volume compared to the sample volume. Therefore, the effect of thermal fluence depression at the irradiation site has been neglected. The extent of non-ideality of epithermal neutron spectrum at the sample irradiation position were determined by using analytical grade-20 μm -thin Au and W foils.

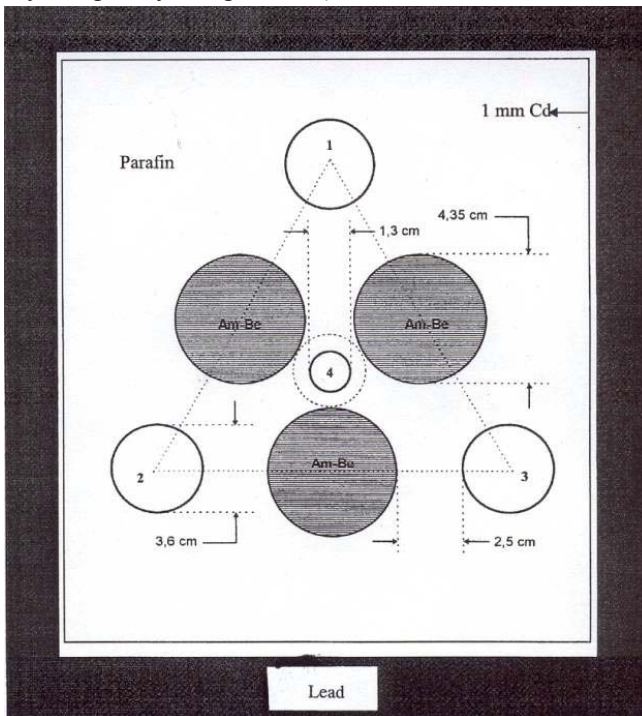


Fig.1 Cross sectional view of 3x592 GBq Am-Be source configuration
Sample irradiation positions in Fig.1 are numbered by Circles 1, 2, 3 and 4.

The irradiations of the samples were carried out within and without a cylindrical cadmium shield case. The 10 diluted samples for each element, Mn and La are individually prepared from the fresh stocks. Each set of 5 samples of MnO_2 and La_2O_3 were irradiated with and without Cd case for the Cd-ratio determinations. The irradiation times for the (n,γ) reactions of ^{55}Mn and ^{139}La were chosen for a period of three to six half lives, yielding enough activity to be measured in a γ -ray counting system. The suitable waiting times were employed to minimize dead time losses and. Dead times were typically less than 0.5 %. The counting times predetermined between 50,000 s and 100,000 s for each measurement was high enough to ensure good statistical quality of data.

The detector used in the measurements was a n-type germanium (REGe) with Be-window and total active volume of 100 cm^3 manufactured by Canberra, Inc. The measured resolution of the Ge detector was 1.80 keV for 1332.5 keV (^{60}Co) and 0.97 keV for 122 keV (^{57}Co) and its relative efficiency was 22.6%. The detector was shielded by lead lined copper sheets on all sides. The absolute photopeak gamma-ray efficiency as a function of energy for the REGe detector in a given sample geometry was determined using the powder radioactive standard containing a mixture of ^{109}Cd , ^{57}Co , $^{123\text{m}}\text{Te}$, ^{51}Cr , ^{113}Sn , ^{85}Sr , ^{137}Cs , ^{60}Co and ^{88}Y radionuclides, obtained from Isotope Products Laboratories Inc. traceable to NIST.

Nuclear decay data, taken from NUDAT database [5], used for determination of the radioactivities and used in the cross section measurements and of the epithermal neutron fluence shaping factor for the neutron irradiation position are given Table 1.

Table 1. Nuclear decay data used for the determination of the radioactivities for the fluence rate, α -epithermal neutron fluence shaping factor and cross section measurements.

Nuclear reaction	Half-life	Detected γ -ray	
		Energy (keV)	Intensity (%)
$^{55}\text{Mn}(n,\gamma)^{56}\text{Mn}$	2.5789 h	846.754	98.9
$^{139}\text{La}(n,\gamma)^{140}\text{La}$	1.6781 d	487.021	45.5
		1596.21	95.4
$^{186}\text{W}(n,\gamma)^{187}\text{W}$	23.72 h	479.550	21.8
		685.73	27.3
$^{197}\text{Au}(n,\gamma)^{198}\text{Au}$	2.69517 d	411.80203	95.58

3. Neutron fluence rate determination

Using the irradiation data for a monitor sample such as Mn or Au, the equivalent 2200 m/s thermal neutron fluence rate can easily be determined by the formula:

$$\Phi_0 = \frac{1}{g\sigma_0 G_{th}} (R_s - R_{s,Cd} F_{Cd}) \quad (1)$$

where R_s is the reaction rate per atom, for an isotope exposed to a mixed thermal and epithermal neutron field (i.e., bare irradiation, $R_{s,Cd}$ is the reaction rate per atom produced within Cd shield case, F_{Cd} is a correction factor, which accounts for the transmission of epithermal neutrons through 1 mm cadmium, and can be taken to be unity, and also g is the Westcott factor, and can also be taken unity for this study because $g(20^\circ\text{C})$ is 1.0004 for ^{55}Mn and 1.00 for ^{139}La [6], G_{th} is thermal neutron self shielding factor.

The reaction rate per atom, R_s and $R_{s,Cd}$ can be calculated by the following equation:

$$R_s \text{ or } R_{s,Cd} = \frac{(A_{sp} \text{ or } A_{sp,e}) F_g M}{\theta N_A \gamma \varepsilon_p} \quad (2)$$

where A_{sp} and $A_{sp,e}$ denote the specific activities obtained after a bare and Cd covered isotope irradiation, and they can be determined as follows:

$$A_{sp} \text{ or } A_{sp,e} = \frac{N_p / t_m}{w SDC} \quad (3)$$

where the nuclear parameters in Eq.2 and in Eq.3 are:

N_p net number of counts under the full-energy peak collected during measuring time, t_m ,

w weight of irradiated element,

$S = 1 - e^{-\lambda t_{irr}}$, saturation factor with λ =decay constant, t_{irr} = irradiation time,

$D = e^{-\lambda t_d}$ decay factor; t_d = decay time,

$C = \frac{1 - e^{-\lambda t_m}}{\lambda t_m}$, measurement factor correcting for decay during the

measuring time, t_m ,

M atomic weight,

θ isotopic abundance,

N_A Avogadro's number,

γ absolute gamma-ray emission probability,

ε_p full-energy peak detection efficiency,

F_g correction factor for gamma ray attenuation.

The correction factor for gamma ray attenuation in the sample at a given gamma ray energy at a fixed geometry for the case of a cylinder, coaxially positioned with the detector, is given by:

$$F_g = \frac{1 - e^{-\mu \rho x}}{\mu \rho x} \quad (4)$$

where μ is the total mass attenuation coefficient (cm^2/g) for the compounds used, taken from XCOM photon cross sections database of Berger and Hubbel [7], ρ is the density of sample (g/cm^3) and x is the sample thickness (cm).

The measured thermal and epithermal fluence rates of the used irradiation hole (labeled as No.1 in Fig.1) of the $3 \times 592 \text{ GBq } ^{241}\text{Am-Be}$ neutron source, are given in Table 2.

Table 2. The results for the thermal and epithermal fluence rates of the used irradiation hole of the $3 \times 592 \text{ GBq } ^{241}\text{Am-Be}$ neutron source

No	Thermal neutron fluence rate, Φ_0 ($n \cdot \text{cm}^{-2} \text{s}^{-1}$) $\times 10^4$	Epithermal neutron fluence rate, Φ_e ($n \cdot \text{cm}^{-2} \text{s}^{-1}$) $\times 10^3$	Thermal to epithermal fluence ratio, $f = \Phi_0 / \Phi_e$
1	1.60 ± 0.07	1.45 ± 0.05	11.03 ± 0.61
2	1.59 ± 0.08	1.43 ± 0.05	11.12 ± 0.68
3	1.54 ± 0.13	1.46 ± 0.06	10.55 ± 0.99
4	1.56 ± 0.12	1.48 ± 0.06	10.54 ± 0.92
Average	1.57 ± 0.21	1.46 ± 0.11	10.81 ± 1.63

4. Determination of thermal neutron cross section by using a single standard material

In the present work, the thermal neutron cross section for the reaction $^{139}\text{La}(n,\gamma)^{140}\text{La}$ has been determined relative to that for the $^{55}\text{Mn}(n,\gamma)^{56}\text{Mn}$ monitor reaction. The thermal neutron cross section, $\sigma_{0,x}$ for the (n,γ) reaction of interest with respect to Eq.1, is calculated as:

$$\sigma_{0,x} = \frac{(R_s - R_{s,Cd})_x}{(R_s - R_{s,Cd})_{Mn}} \cdot \frac{(G_{th} g)_{Mn}}{(G_{th} g)_x} \cdot \sigma_{0,Mn} \quad (5)$$

where x corresponds to La. The reaction rates R_s and $R_{s,Cd}$ for ^{55}Mn monitor and ^{139}La isotope are determined from Eq.2, after a bare and Cd covered sample irradiations. The thermal neutron self shielding factors G_{th} , given in Table 4, have been calculated for the relevant reactions according to the self shielding correction procedure described in section 7.1.

5. α - shape factor determination in the $1/E^{1+\alpha}$ epithermal $^{241}\text{Am-Be}$ source-neutron spectrum

The extent of non-ideality of epithermal fluence shape, α -factor at the sample irradiation position of the used irradiation hole of the $^{241}\text{Am-Be}$ neutron sources

immersed in paraffin, was experimentally determined by using the dual monitor method suggested by De Corte et al [8,9], using the measured Cd ratios, R obtained from $^{197}\text{Au}(n,\gamma)^{198}\text{Au}$ and $^{186}\text{W}(n,\gamma)^{187}\text{W}$ reactions, in which 20 μm thin Au and W foils were used.

$$\frac{(R-1)_{\text{Au}}}{(R-1)_{\text{W}}} = \frac{\left[\left(\frac{I_0}{\sigma_0} \right)_{\text{W}} - 0.426 \right] \left(\bar{E}_{r,\text{W}} \right)^{-\alpha} + \frac{0.426}{(2\alpha+1)E_{\text{Cd}}^\alpha}}{\left[\left(\frac{I_0}{\sigma_0} \right)_{\text{Au}} - 0.426 \right] \left(\bar{E}_{r,\text{Au}} \right)^{-\alpha} + \frac{0.426}{(2\alpha+1)E_{\text{Cd}}^\alpha}} \quad (6)$$

The reference values of I_0/σ_0 for ^{197}Au and ^{186}W are used [9]. α -epithermal neutron spectrum shape factor is found to be 0.560 ± 0.002 for the sample irradiation position(labeled no.1 in Fig. 1.) by solving Eq. 7 graphically, by means of a computer.

6. Determination of resonance integral cross section

In an ideal $1/E$ epithermal neutron spectrum, the resonance integral cross section, I_0 including $1/v$ tail of thermal neutron spectrum, tabulated in literature is defined by the following relation:

$$I_0 = \int_{E_{\text{Cd}}=0.55\text{eV}}^{\infty} \frac{\sigma(E)}{E} dE \quad (7)$$

where $\sigma(E)$, is the cross section as a function of energy E , E_{Cd} is the cadmium cut-off energy. It has been shown by De Corte et al. [8] that the resonance integral definition I_0 according to Eq.7 is not valid in a non-ideal, real epithermal neutron spectrum and that such a deviating epithermal neutron fluence distribution can be in most cases approximated by $\Phi_e(E) \sim 1/E^{1+\alpha}$ which is epithermal neutron flux per unit $(E^{-\alpha}/-\alpha) \cdot 1\text{eV}^\alpha$ of neutron energy interval. Accordingly, a resonance integral $I_0(\alpha)$ replacing by Eq.7 for a $1/E^{1+\alpha}$ real epithermal spectrum is defined as [8-10]:

$$I_0(\alpha) = \int_{E_{\text{Cd}}}^{\infty} \frac{\sigma(E)(1\text{eV})^\alpha}{E^{1+\alpha}} dE \quad (8)$$

where α is an energy independent correction factor for spectrum shape, which can be positive or negative, depending on the irradiation system configuration (moderator material, geometry of irradiation site, etc.), $I_0(\alpha)$ is the resonance integral, which should be used in the calculation of the epithermal activation in a particular irradiation position, characterized by α , and the term $(1\text{ eV})^\alpha \equiv 1$ is omitted.

It has been shown that the relationship between I_0 , as tabulated in literature, and $I_0(\alpha)$ for the conversion is given by [9]:

$$I_0(\alpha) = (1\text{eV})^\alpha \left[\frac{I_0 - 0.426 \sigma_0}{(\bar{E}_r)^\alpha} + \frac{0.426 \sigma_0}{(2\alpha + 1)(E_{Cd})^\alpha} \right] \quad (9)$$

where \bar{E}_r , effective resonance energy (eV), as defined and tabulated by Moens et al.[11], and the term $(I_0 - 0.426 \sigma_0)$ represent the reduced resonance integral, i.e. with the $1/v$ tail subtracted. The Eq.9 is only valid for $E_{Cd} = 0.55$ eV, since $0.426 = 2(E_0/E_{Cd})^{1/2}$ with $E_0 = 0.025$ eV and $E_{Cd} = 0.55$ eV. The values of effective resonance energy, \bar{E}_r are 412 eV for ^{55}Mn and 76.8 eV for ^{139}La [11]

In a mixed thermal and $1/E^{1+\alpha}$ epithermal neutron field, the ratio of the epithermal neutron fluence rate per unit of $(E^{-\alpha}/\alpha)$ interval to thermal neutron fluence rate can be written as:

$$f = \frac{\Phi_0}{\Phi_e} = [R - 1] \frac{I_0(\alpha)}{g\sigma_0} \frac{G_{\text{epi}}}{G_{\text{th}}} \quad (10)$$

where R is the cadmium ratio at the irradiation position, defined by $R = (A_{sp}/A_{sp,e})$, using specific activities without Cd and with Cd.

The measured $I_0(\alpha)$ value for the $^{139}\text{La}(n,\gamma)^{140}\text{La}$ reaction has been determined relative to that for the $^{55}\text{Mn}(n,\gamma)^{56}\text{Mn}$ reaction as a standard by the following relation:

$$I_0(\alpha)_x = I_0(\alpha)_{\text{Mn}} \frac{g_x \sigma_{0,x}}{g_{\text{Mn}} \sigma_{0,\text{Mn}}} \frac{(R-1)_{\text{Mn}}}{(R-1)_x} \left(\frac{G_{\text{epi}}}{G_{\text{th}}} \right)_{\text{Mn}} \left(\frac{G_{\text{th}}}{G_{\text{epi}}} \right)_x \quad (11)$$

In the determination of resonance integral $I_0(\alpha)_x$, for any isotope under study from Eq. 11, the estimated thermal and epithermal self shielding factors, G_{th} and G_{epi} given in Table 4 and in Table 6, and reference values of $\sigma_{0,\text{Mn}}$, $I_{0,\text{Mn}}$, g_{Mn} are used. Then, the obtained $I_0(\alpha)$ values were converted to I_0 by using Eq.9, and the results are given in Table 8.

7. Neutron self-shielding correction factors

7.1. Thermal neutron self-shielding correction factor

The magnitude of the fluence correction with sufficient precision can be evaluated by making appropriate assumptions:(1) neutrons are considered to be in a Maxwellian distribution with a velocity of 2200 m/s, (2) the neutron fluence can be treated being isotropic. Hence, a neutron self shielding factor, G for a sample is defined as follows:

$$G = \frac{\Phi_{av}}{\Phi_0} \quad (12)$$

where, Φ_{av} is an average fluence rate in the sample and will be always less than Φ_0 which is the incident fluence. The magnitude of self shielding factor depends on the size and shape of the sample. The thermal neutron self-shielding factor G_{th} for a finite cylinder of radius R and length L in an isotropic neutron field can be

calculated in conjunction with macroscopic absorption cross section $\Sigma_a = n\sigma_a$ as follows:[12, 13, 14]:

$$G_{th} = \frac{R \cdot G_{slab} + L \cdot G_{inf\ cyl}}{R + L} \quad (13)$$

where G_{slab} and $G_{inf\ cyl}$ are the self-shielding factors for a slab and an infinite cylinder, respectively.

For a slab:

$$G_{slab} \cong 1 - \frac{\tau}{2} \left[0.9228 + \ln \frac{1}{\tau} \right] \quad (14)$$

For an infinite cylinder with radius R:

$$G_{inf\ cyl} \cong 1 - \frac{4}{3} \tau \quad (15)$$

with $\tau = N\sigma t$, where N = atom density(atoms/cm³), t =slab thickness(cm) or t =R cylinder radius, and σ =average thermal neutron cross section. The sample shape parameter, τ for a cylinder with a sample volume(V), and its surface area(S), is defined as

$$\tau = \frac{2V}{S} \Sigma_a = \frac{R \cdot L}{R + L} \Sigma_a \quad (16)$$

The composition weighted macroscopic cross section, Σ_a can be related to the known constituents of a sample and it can be calculated using the tabulated elemental values given in Table 3 by following relation:

$$\Sigma_a = \frac{\sqrt{\pi}}{2} \sum_i N_i \sigma_{0i} \quad (17)$$

where Σ_a is total macroscopic absorption cross-section of the compound or mixture (Maxwellian average),

N_i is number of absorbing nuclides per cm³ of i^{th} component in the compound or mixture, and σ_{0i} is absorption cross section with 2200 m/s neutron velocity for the i^{th} component.

Since the neutrons from the isotopic neutron sources at the room temperature, $T_0=20.43$ °C for irradiation purposes were used instead of reactor neutrons, the averaged absorption macroscopic cross section would become independent of neutron temperature. However, the effect of neutron scattering in the sample has been taken into account by applying the necessary correction for this effect given by the following formula [12,13]:

$$G_{th}^* = \frac{G_{th}}{1 - \frac{\Sigma_s}{\Sigma_t} (1 - G_{th})} \quad (18)$$

where G_{th}^* is the thermal self-shielding factor corrected for scattering, $\Sigma_t = \Sigma_a + \Sigma_s$, Σ_s are total and scattering macroscopic cross-sections, respectively. The thermal neutron self-shielding factors, G_{th}^* , including the scattering effect for Mn and La were calculated from Eq 18. Typical values of G_{th}^* for the samples investigated are given in Table 4.

Table 3. Absorption, scattering and total microscopic cross sections for thermal neutrons, and atomic weights for elements of interest

Element	Atomic Weight, M (g/mol)	Microscopic cross sections (b)		
		Absorption, σ_a	Scattering, σ_s	Total, σ_t
${}_8\text{O}$	15.9994	$1.9 \cdot 10^{-4}$	3.78	3.780
${}_{25}\text{Mn}$	54.9380	13.41	2.17	15.58
${}_{57}\text{La}$	138.905	8.93	10.13	19.06

Table 4. The calculated thermal neutron self shielding factors for MnO_2 , and La_2O_3 .

	Samples used	
	MnO_2	La_2O_3
Molecular weight, W (g.mol $^{-1}$)	86.9368	325.8092
Mass of the irradiated sample, m (g)*	0.035	0.047
Thermal self shielding factor, G_{th} from Eq.13	0.9978	0.9989
Thermal self shielding factor including scattering, G_{th}^* from Eq.18	0.9988	0.9996

*A typical value for an example irradiation.

7.2 Epithermal neutron self shielding correction factor

The epithermal neutron self-shielding factor, G_{epi} is defined by

$$G_{epi} = \frac{I_{eff}}{I_0} \quad (19)$$

where I_0 , I_{eff} are the infinitely diluted resonance integral and the effective resonance integral, respectively. I_{eff} can be calculated by using the sum of symmetric Breit-Wigner line shape arising from the various resonances, as follows [15]:

$$I_{eff} = I_{1/v} + \frac{\pi}{2} \sum_i \left(\frac{\Gamma_\gamma}{E_r} \right)_i \frac{\sigma(E_{ri})}{\sqrt{1 + 2Nd\sigma(E_{ri})}} \quad (20)$$

and similarly, I_0 can also be calculated as follows :

$$I_0 = I_{1/v} + \frac{\pi}{2} \sum_i \left(\frac{\Gamma_\gamma}{E_r} \right)_i \sigma(E_{ri}) \quad (21)$$

where,

E_{ri} i^{th} neutron resonance energy,

$\Gamma_{\gamma i}$ the probability per unit time interval for the compound nucleus to de-excite by emitting one or more photons for i^{th} resonance,

$\sigma(E_{ri})$ total cross-section at maximum of i^{th} resonance,

N number of absorbing nuclides per cm^3 and,

d mean chord length ($=2V/S$), where, V , S denote volume and total surface of cylinder, respectively,

$I_{1/v}$ $1/v$ contribution ($=0.43 \sigma_0$ for $E_{Cd}=0.55$ eV for cylinder box with 1 mm wall thickness).

The epithermal neutron self-shielding factors, G_{epi} for the cylindrical sample geometry were calculated by using the characteristic resonance parameters given in Table 5, and material constants given in Table 6.

Table 5. Some characteristic resonance parameters of main resonances for ^{55}Mn and ^{139}La [16].

Nuclide	Resonance Energy $E_r(\text{eV})$	Radiative width of the resonance, $\Gamma_\gamma(\text{eV})$	Total width of the resonance, $\Gamma(\text{eV})$	Cross section at the resonance energy, $\sigma(E_r)$ (b)
^{55}Mn	337.3	0.31	22.3	3287
	1099	0.31	15.7	1439
	2327	0.34	395	675.7
^{139}La	72.30	0.054	0.088	6251
	617.2	0.031	0.057	1118
	875.4	0.023	0.044	799.6
	962.9	0.030	0.049	485.5
	1179	0.051	2.163	958.8

Table 6. Calculated epithermal neutron self-shielding factors.

Element	Sample	Sample mass, m (g)	Target nuclide	Abundance θ (%)	Number of nuclides per cm^3 , $N \times 10^{20} (\text{cm}^{-3})$	Epithermal neutron self shielding factor [♠] , G_{epi}
Mn	MnO_2	0.035	^{55}Mn	100	2.058	0.916
La	La_2O_3	0.047	^{139}La	99.909	1.535	0.848

♠: These values are for the specified sample amounts.

8. Results and discussion

The thermal neutron cross section for the $^{139}\text{La}(n,\gamma)^{140}\text{La}$ reaction has been obtained relative to the reference cross section value of 13.3 ± 0.1 b of $^{55}\text{Mn}(n,\gamma)^{56}\text{Mn}$ reaction. The experimental uncertainties for the ^{139}La and ^{55}Mn are given in Table 7. The main sources of the uncertainties are due to statistical errors (0.38-0.39%), detection efficiencies (2.52-2.75%) and other errors including some corrections. The data obtained with different irradiation and counting times of activation samples were relatively close to each other, and the difference of the results is within about 1.2% for La. There existed a consistency among the measured data.

The obtained thermal cross section value for $^{139}\text{La}(n,\gamma)^{140}\text{La}$ reaction is $\sigma_0=9.27 \pm 0.37$ b given in Table 8 and compared with experimental and evaluated data. The present result for thermal cross section for the $^{139}\text{La}(n,\gamma)^{140}\text{La}$ reaction is in good agreement with the measurements of Holden [17] and Heft [15], and is close to within 1 to 5% with the values obtained by Gleason [18], Ryves [19], Mughabghab et al. [3], De Corte et al. [20] and Kafala et al. [21], but disagrees with the measurements of Steinnes [22] and Lyon [23] by 14.4-17.2. The present value agrees within 3-4% with the evaluated values of JENDL-3.2[16], IAEA[24] and BNL[25].

The value of resonance integral for the $^{139}\text{La}(n,\gamma)^{140}\text{La}$ reaction has been obtained relative to the reference value of 14.0 ± 0.3 for the $^{55}\text{Mn}(n,\gamma)^{56}\text{Mn}$ reaction by assuming the cadmium cut-off energy of 0.55 eV. The obtained result for the resonance integral cross section for the $^{139}\text{La}(n,\gamma)^{140}\text{La}$ reaction is 12.16 ± 0.60 b and this value disagrees with the measurements of Ryves[19], Harris et al. [26] and Alian [27] by 6-40.6%. However, the present result agrees well the recently reported value obtained by Holden[17] by 0.13%, assuming Cd cut-off energy of 0.50 eV. The precision of the present measurement is higher than that of Holden[17]'s result, but the precision of the result obtained by Kafala et al.[21] is two times better than those of the results in the surveyed literature, given in Table 8.

In conclusion, the present results for the $^{139}\text{La}(n,\gamma)^{140}\text{La}$ reaction obtained by the activation method show that the thermal neutron cross section and the resonance integral for the isotopes can be determined with sufficient accuracy by using small amounts of powder samples similar to the foils, when the necessary corrections are made for the results. Manganese having the good nuclear parameters can be used a standard material in the activation method instead of ideal monitor- gold employed in the analysis of the most reactions.

Table 7. Experimental uncertainties for the thermal neutron cross section and resonance integral cross section measurements.

<i>Thermal neutron cross section measurements</i>		
<i>Uncertainties due to</i>	<i>Uncertainties (%)</i>	
	$^{139}\text{La}(n,\gamma)^{140}\text{La}$	$^{55}\text{Mn}(n,\gamma)^{56}\text{Mn}$
Statistical error*	0.38	0.39
Detection efficiency,	2.52	2.75
Mass of sample	0.01	0.01
Half-life	0.018	0.004
Isotopic abundance	0.0005	---
Branching ratio	1.13	0.30
Self-shielding factor	0.01	0.01
g-factor	< 0.05	< 0.05
Monitor thermal neutron cross section [9,8]	--	0.75
Total error (in quadrature)	2.79	2.89

<i>Resonance integral cross section measurements</i>		
<i>Uncertainties due to</i>	<i>Uncertainties (%)</i>	
	$^{139}\text{La}(n,\gamma)^{140}\text{La}$	$^{55}\text{Mn}(n,\gamma)^{56}\text{Mn}$
Cadmium ratio	1.58	1.60
Self-shielding factor	0.60	0.20
g-factor	< 0.05	< 0.05
Reference thermal neutron cross section	0.448	0.75
Monitor resonance integral cross section [5, 21]	--	2.14
α -shape parameter	0.89	1.20
--	--	--
Total error(in quadrature)	1.96	4.56

*Errors are based on counting statistics of $\pm 1.65 \sigma$ (at 90 % confidence level)

Table 8. Thermal neutron cross section and resonance integral cross section for $^{139}\text{La}(n,\gamma)^{140}\text{La}$ reaction.

Year	References	Thermal neutron cross section, σ_0 (b)	Resonance integral cross section, I_0 (b)	Cadmium cut-off energy, E_{Cd} (eV)
	This Work	9.27 ± 0.37	12.16 ± 0.60	0.55
1999	Holden [17]	9.2 ± 0.2	12 ± 1	0.50
1997	Kafala et al. [21]	9.67 ± 0.30	11.6 ± 0.2	0.55
1997	JENDL-3.2 [16]	8.930	11.8	0.50
1989	De Corte et al. [20]	9.43 ± 0.09	11.6	---
1987	IAEA [24]	8.93 ± 0.04	12.2 ± 0.8	---
1981	Mughabghab et al. [3]	8.93 ± 0.04	11.8 ± 0.8	0.50
1978	Heft [10]	9.18 ± 0.05	12.6 ± 0.6	0.50
1978	Takiue [28]	8.63 ± 0.34	---	---
1975	Gleason [18]	9.15 ± 0.25	12.5 ± 0.4	0.50
1975	Steinnes [22]	11.2 ± 0.5	---	0.50
1974	V.D.Linden et al. [29]	11.6 ± 0.7	---	0.55
1973	BNL [25]	9.0 ± 0.3	12.2 ± 0.6	0.50
1973	Alian [27]	---	17.1	0.50
1972	Steinnes [30]	---	11.8 ± 1.2	0.50
1971	Ryves [19]	9.03 ± 0.33	11.4 ± 0.8	0.50
1971	De Corte [31]	---	11.0	0.50
1968	Orvini [32]	---	10.8 ± 1.1	0.55
1967	Brien [33]	9.5 ± 0.5	11.2 ± 0.6	0.54
1960	Lyon [23]	8.10	---	---
1957	Cummins [34]	9.1 ± 0.2	---	---
1951	Pomerance [35]	8.8 ± 0.44	---	---
1951	Benoist [36]	8.35 ± 0.10	---	---
1950	Harris et al. [26]	---	13.2	0.50

References

1. Ryves, T.B and Zieba, K.J. J.: Phys: Math., Nucl. Gen., 7(18), 2318 (1974).
2. Neutron fluence measurements, Technical report series no: 107, IAEA, Vienna, 1970.
3. Mughabghab, et al.: *Neutron Cross Section from Neutron Resonance Parameters and Thermal Cross Sections*, Academic Press, New York, 1981.
4. Goldstein, H., et al.: Recommended definitions for resonance integral cross section, Report E.A.N.D.C., 12, 1961.

5. Nuclear Data Retrieval, <http://www.nndc.bnl.gov> (NuDat).
6. El. Nimr, T., et al.: J. Radioanal. Chem., **67**(2), 421 (1981).
7. Berger, M. J., Hubbell, J. H.: XCOM Photon Cross Sections Database, NBSIR 87-3597, 1987.
8. De Corte, F., et al.: J. Radioanal. Chem., **52**(2), 305 (1979).
9. De Corte, F., et al.: J. Radioanal. Chem., **52**(2), 295 (1979).
10. Heft, R. E.: A consistent set of nuclear-parameter values for absolute instrumental neutron activation analysis, Conf. on Computers In Activ. Analysis, Mayaguez, Puerto Rico, 1978, p. 495.
11. Moens, L., et al.: J. Radioanal. Chem., **52**(2), 379 (1979).
12. Gilat, J., Gurfinkel, Y.: Nucleonics, **21**(8), 143 (1963).
13. Fleming, R. F.: Int. J. Appl. Radiat. Isot., **33**, 1263 (1982).
14. Shakir, N. S., Jervis, R. E.: J. Radioanal. Nucl. Chem., **248**(1), 61 (2001).
15. Beckurts, K., Wirtz, K.: *Neutron Physics*, Springer, Berlin, 1964
16. Fukahori, T., et al.: *JENDL-3.2*, JAERI-Data/Code 97-044, 1997.
17. Holden, N. E.: Neutron scattering and absorption properties (revised 1996) In: *CRC Handbook of Chemistry and Physics* (D. R. Lide, ed.), 79 th ed., CRC Press, New York 1999.
18. Gleason, G.: Radiochem. and Radioanal. Letters, **23**, 317 (1975).
19. Ryves, T. B.: J. Nucl. Energy, **25**, 129 (1971).
20. De Corte, F., et al.: Radioanal. Nucl. Chem., **133**, 43 (1989).
21. Kafala, S. I., et al.: J. Radioanal. Nucl. Chem., **215**(2), 193 (1997).
22. Steinnes, E.: J. Inorg. Nucl. Chem., **37**, 1591 (1975).
23. Lyon, W. S.: Nucl. Sci. Eng., **8**, 378 (1960).
24. Handbook of nuclear activation data, Tech. Rept. series no: 273, IAEA, Vienna, 1987.
25. Neutron cross-sections, BNL-325, 3rd ed., Vol.1, 1973.
26. Harris, S. P., et al.: Phys. Rev., **79**, 11 (1950).
27. Alian, A., et al.: Radioanal. Chem., **15**, 535 (1973).
28. Takiue, M., Ishikawa, H.: Nucl. Instrum. Methods in Physics Res., **148**(1), 157 (1978).
29. Van Der Linden, R., et al.: J. Radioanal. Chem., **20**, 695 (1974).
30. Steinnes, E.: J. Inorg. Nucl. Chem., **34**, 2699 (1972).
31. De Corte, F., et al.: Radioanal. Chem., **9**, 9 (1971).
32. Orvini, E., et al.: J. Inorg. Nucl. Chem., **30**, 1353 (1968).
33. Brien, H. A., et al.: J. Inorg. Nucl. Chem., **29**, 584 (1967).
34. Cummins, J. D.: A.E.R.E. Harwell Reports, 2333, 1957.
35. Pomerance, H.: Thermal neutron capture cross sections, Phys. Rev., **83**, 641 (1951).
36. Benoist, P., et al.: Journal de Physique, **12**, 584 (1951).

MEASUREMENT OF TIME STRUCTURE AND THE INTERNAL BEAM INTENSITY AT THE CYCLOTRON

A. Arzumanov, M. Gorkovets, V. Koptev

Institute of Nuclear Physics, Almaty, 480082, Kazakhstan

Abstract.

During last years the application of the cyclotron has been increased essentially. More high beam quality and more operative tuning of the cyclotron were needed.

To obtain current information on beam acceleration at the cyclotron six inductive pick up probes were mounted in the dee. These probes make possible to determine the phase of the ion beam and phase wide on the different radii. Simultaneously internal beam intensity is determined with these probes.

In the article design of the pick up probes and the results of beam parameters measurement are presented. The accuracy of phase measurement is equal to 0.35° and measurement of the time duration of the ions bunch is equal to 0.5 ns.

The variable energy isochronous cyclotron U-150M had been put into operation in 1972. Different modes of operation are based on the magnetic field measurements and calculations of beam dynamic performed at that time. Two probes were mounted in the cyclotron for diagnostic of internal beam: first one is located between dees in the direction of resonators (it can be moved along the radius), second one is located behind the exit channel. These probes cannot give full information about ion acceleration process from the center to the final radius.

In connection with new irradiation works demanding more bombarding accuracy inside the vacuum tank of the cyclotron it is necessary to optimize the process of acceleration mode. In order to get phase information along the cyclotron radius six pickup probes have been mounted in the right cyclotron's dee. The probes are located along the radius at points: 31 cm, 38 cm, 45 cm, 52 cm, 58 cm and 65 cm. The accuracy of probe mounting is equal to $\pm 0,5$ cm.

Phase probes

6 identical pickups are made as parts of a strip line (fig.1.).

The probe's iterative impedance is equal to $Z=50$ Ohm, bandpass – 1 GHz, ripple – 3 db. The design of probe allows to mount it on the lower surface of the right dee. The probes are connected with measurement devices by equal length coaxial cable. Difference of cables' electrical size is not more than ± 50 psec, or it is equal to $5'$ (in phase degree) at 30 MeV protons mode.

Scheme of measurement of the beam phase is shown in the fig.2.

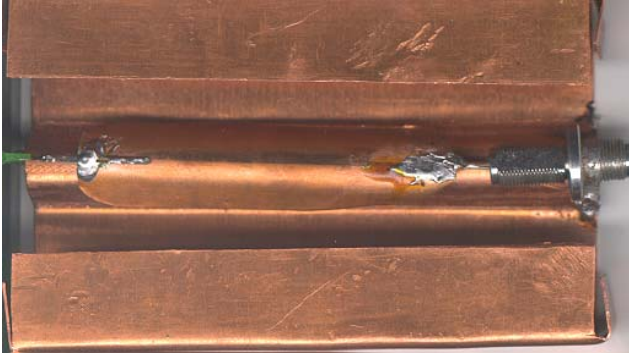


Fig.1. Phase probe.

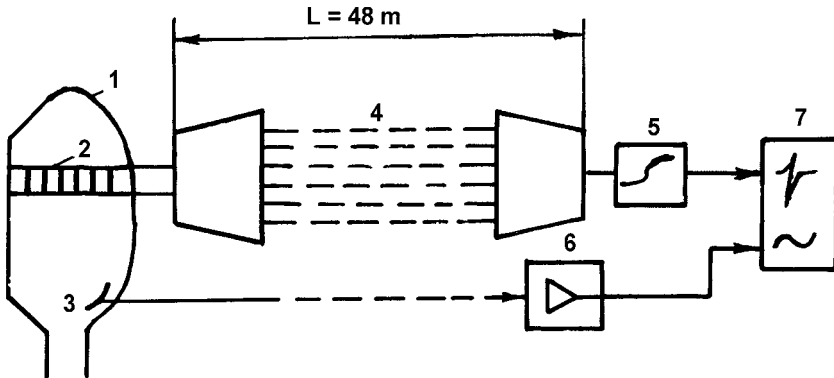


Fig.2. Scheme of phase beam measurement.

1 – dees, 2 – pickups, 3 – probe of accelerating voltage, 4 – feeders,
5 – filter (0 – 21 MHz), 6 – amplifier with delay, 7 – measurement device.

In order to get real phase information multiplexers and commutators were excepted. The oscilloscope TDS-380 with a time step of 20 psec was used as a measuring instrument. Output voltage of one pickup and accelerating voltage probe are shown in the fig.3. The accuracy of phase measurement is equal to 0.35° .

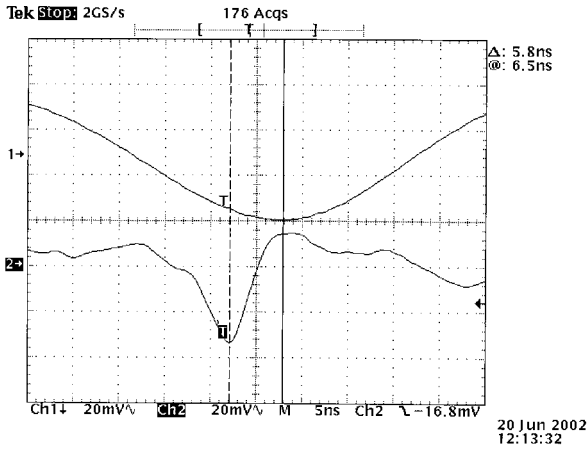


Fig.3. Measured signals of pickup (2) and accelerating voltage probe (1).

Measurements

Measurements of the accelerated ion beam phase were carried out at the 22 MeV protons mode of operation ($f=15.7$ MHz, $U_{\text{left}}/U_{\text{right}}=45/43$ kV, $I=20$ μ A of the internal beam). The sinusoidal signal of accelerating voltage probe fed one channel of the oscilloscope while signals of pickups fed second channel by turns. Since the signal of accelerating voltage has a stable phase and amplitude, it was used as reference signal. As a calibration method was chosen an accelerating zero phase for the first pickup. It means that the peak of a pulse from the 1-st pickup marked by the cursor was combined by means of delay line with the maximum amplitude of accelerating voltage, marked also by the cursor. In fig.4 it is shown the beam phase changes relative to accelerating rf-voltage along the cyclotron radius.

Dependence of average magnetic field vs. radius determines beam phase change. For example, in fig 5 dependence of average magnetic field vs. radius for 30 MeV protons mode is shown. According to this field the beam phase changes, as it is shown in fig 6. One can distinctly see isochronous acceleration in the range of 30 cm – 54 cm. The measured phase change (fig 7) reflects the field configuration in the experiment.

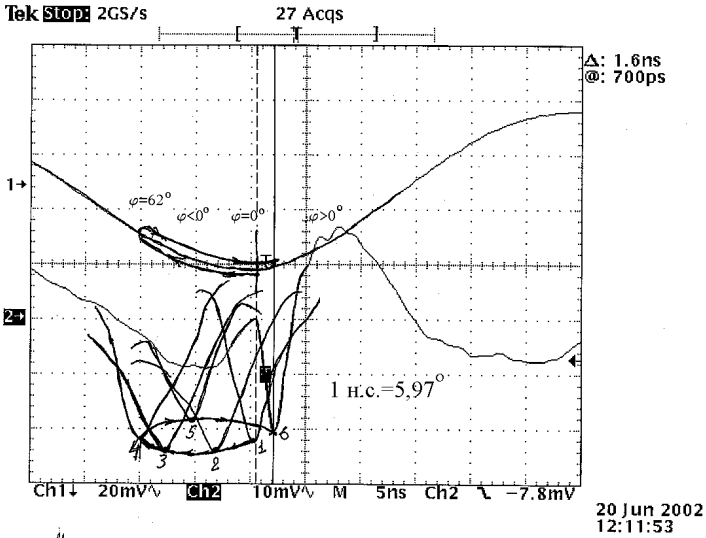


Fig.4. Change of phase as pickups' output voltage and the projection of pickups' signals to the reference one.

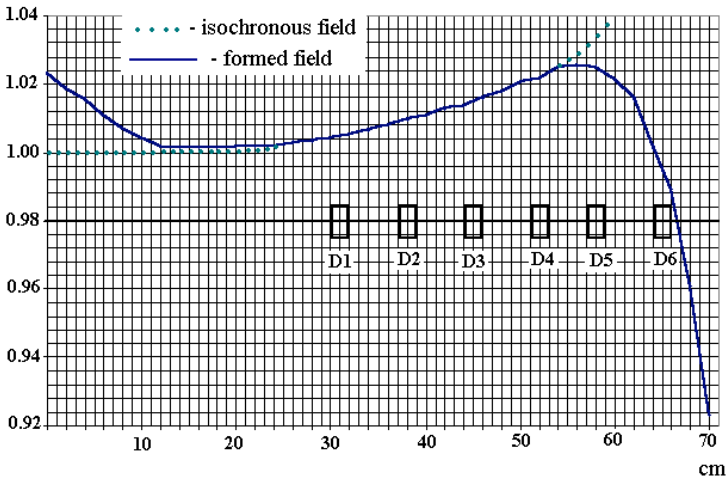


Fig.5. Dependence of average magnetic field of 30 MeV protons mode versus radius. D1, D2, D3, D4, D5, D6 – pickup probes.

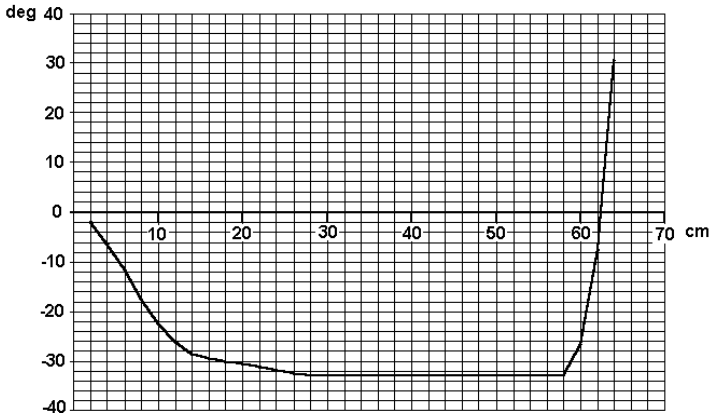


Fig. 6. Dependence of RF phase versus radius.

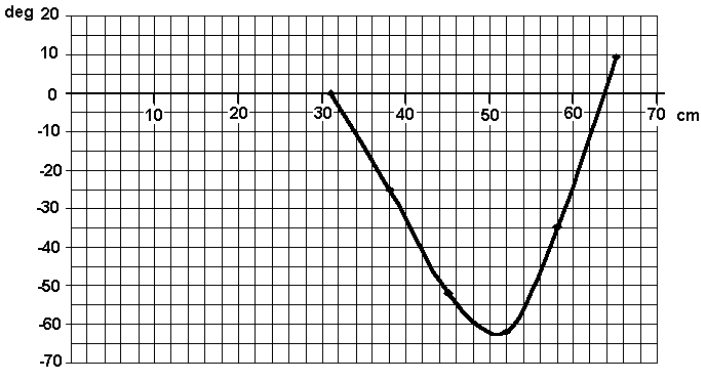


Fig. 7. Dependence of measured beam phase versus radius.

Conclusion

Pickup probes, mounted in dees, give information about the beam phase change along radius in accordance with formed magnetic field of operational mode. In order to provide optimal cyclotron operation it is necessary to create a control system of pickups more than 6. It will allow to correct isochronous field to given mode and increase internal and external beam parameters.

References

1. Arzumanov A.A., Butishev V.N. et.al. Status of the Alma-Ata Isochronous Cyclotron. –10-th Int. Conf. Cycl. and their Appl., East Lansing (USA), 1984, pp. 476-482.